Supporting Information

A versatile switchable dual-modal colorimetric and photoelectrochemical biosensing strategy *via* light-controlled sway of signal-output transverter

Lingling Zhu,[‡a] Tianxiang Wei,[‡b] Renzhong Yu,[a] Wenwen Tu*[ac] and Zhihui Dai*[a]

[a]Jiangsu Collaborative Innovation Center of Biomedical Functional Materials and Jiangsu Key Laboratory of Biofunctional Materials, College of Chemistry and Materials Science, Nanjing Normal University, 210023, P. R. China.

[b]School of Environment, Nanjing Normal University, Nanjing, 210023, P. R. China.

[c]Huaian Research Institute of Nanjing Normal University, Huaian, P. R. China.

*Tel./Fax: +86-25-85891051. E-mail: wwt@njnu.edu.cn (W. Tu), daizhihuii@njnu.edu.cn (Z. Dai).

‡ These authors contributed equally to this work.

List of contents:

1. Experimental procedures

1.1. Materials and reagents: Zinc nitrate hexahydrate ($Zn(NO_3)_2 \cdot 6H_2O$), iron nitrate nonahydrate ($Fe(NO_3)_3 \cdot 9H_2O$), hydrochloric acid (HCl, 36 wt%), acetone (C_3H_6O), nitric acid (HNO_3, 65 wt%), ammonia water (25 wt%) and hydrogen peroxide (H_2O_2, 30 v%) were obtained from Sinopharm Chemical Reagent Co. Ltd. 2'-azino-bis(3-ethylbenzothiazoline-6-sulfonic acid) (ABTS) was bought from Aladdin. Tris (hydroxymethyl) aminomethane (Tris) was purchased from Alfa Aesar. Mercaptoethanol (MCH), 1-Ethyl-3-[(3-dimethylamino)-propyl)] carbodiimide (EDC), N-hydroxysuccinimide (NHS) were obtained from Sigma-Aldrich. Streptavidin-horseradish peroxidase (Strep-HRP) was purchased from Shanghai Sangon Biotechnology Co. Ltd. The chemical reagents were analytical grade. Indium tin oxide (ITO) glass as the working electrode was produced in Jintan Kondrk Photoelectric Science & Technology Co. Ltd. Ultrapure water was obtained through a microporous water purification system (≥18 MΩ·cm, Millipore SAS Corporation, France). The washing solution was 10 mM Tris-HCl buffered solution (pH 7.4). DNA was synthesized by Shanghai Sangon Biotechnology Co. Ltd. with base sequences as follows:

Probe DNA: 5'-COOH-CTC CCC GAC CCA ATT TCC ACC TTC G-3',

Capture DNA: 5'-biotin-CGA AGG TGG A-3',

Complementary target DNA (tDNA): 5'-CGA AGG TGG AAA TTG GGT CGG GGA G-3',

Single base mismatched DNA (S1): 5'-CGA A*A*G TGG AAA TTG GGT CGG GGA G-3',

Double base mismatched DNA (S2): 5'-CGA *C*GG TGG AAA TTG GGT CG*A* GGA G-3',

Non-complementary DNA (S3): 5'-GAG GGC CTG CAG GAT CAT TGG CTT T-3'.

1.2. Apparatus: The field emission transmission electron microscope (FETEM) test was performed using the Tecnai G2 F20 field emission transmission electron microscope (FEI, USA). X-ray powder diffraction (XRD) was executed the diffractometer with graphite monochromatized Cu Ka radiation (D/max 2500 VL/PC, Japan). Fourier transform infrared

(FTIR) spectra were obtained with ALPHA II (Bruker, Germany), equipped with a platinum ATR sampler. Spectra were recorded at room temperature in the range of 4000-400 cm^{-1}. The amide I band was processed by the fitting program, having a linear baseline between 1700 and 1550 cm^{-1}. The component peaks were fitted with Gaussian bands. Ultraviolet-visible (UV-vis) absorption was completed on a Cary 60 spectrophotometer (Agilent, USA) and a Multiskan GO microplate reader (Thermo Fisher Scientific, USA). The X-ray photoelectron spectroscopy (XPS) measurement was obtained on a Thermo Fisher Scientific ESCALAB Xi+ system. Scanning transmission electron microscopy (STEM) image and the elemental mapping analysis were performed on JEM-2100F (JEOL, Japan). Electrochemical impedance spectroscopy (EIS) was obtained using a Nova 1.8 software controlled Autolab potentiostat/constant current regulator PGSTAT302N (Metrohm, the Netherlands). The electrolyte solution was 5 mM $K_3Fe(CN)_6/K_4Fe(CN)_6$ (1:1) solution containing 0.1 M KCl. At an open circuit voltage, the frequency was from 0.1 Hz to 100 kHz and the exchange voltage amplitude was 10 mV. PEC measurements were performed at a Zahner PEC workstation (Zahner, Germany). The whole tests were operated using a conventional three-electrode system at room temperature: A modified ITO electrode with a round area of 0.25 cm^2 (surface resistance, 20-25 $\Omega \cdot m^{-2}$) was used as the working electrode, the platinum wire was chosen as the auxiliary electrode, and saturated calomel electrode was selected as the reference electrode.

1.3. Synthesis of $ZnFe_2O_4$ nanoparticles: Hydrothermal method was applied to synthesize $ZnFe_2O_4$ nanoparticles (NPs), which was based on the previous report.[1] $Zn(NO_3)_2 \cdot 6H_2O$ and $Fe(NO_3)_3 \cdot 9H_2O$ were entirely dissolved in 60 mL of ultrapure water. The concentrations were 20 mM ($Zn(NO_3)_2 \cdot 6H_2O$) and 40 mM ($Fe(NO_3)_3 \cdot 9H_2O$), respectively. Ammonia water was added dropwise to the solution for adjusting the pH to 10 and then it formed a well-dispersed red-brown suspension. Afterward, the obtained solution was transferred to a 100 mL polytetrafluoroethylene autoclave and sealed. It was heated at 170 °C for 6 hours, then naturally

cooled down to room temperature. The brown precipitate was collected, then transferred to a new beaker and rinsed carefully three times with ultrapure water. In order to minimize soft aggregation of $ZnFe_2O_4$ NPs, concentrated nitric acid (65 wt%) and ultrapure water were added in a volume ratio of 1:3 and stirred with a magnetic stirrer, the process was repeated three times. Stirring time was 30 min (the first time), 20 min (the second time) and 10 min (the third time). Finally, the prepared sample was dried in a vacuum oven at 60 °C overnight.

1.4. Fabrication of the dual-modal colorimetric and PEC biosensor: A piece of bulked ITO (sheet resistance 20-25 Ω/square) was incised to small pieces of rectangular ITO. Before modification, the working electrode (ITO) was first ultrasonically cleaned with acetone, then sonicated with 1 M NaOH/ethanol mixed solution (v/v, 1:1), and finally treated with ultrapure water, dried at 60 °C. Then, the nonconductive rubberized fabric with hollow-carved circle (the diameter was 0.56 cm) was pasted on the small piece of rectangular ITO to obtain the modified electrode (Fig. S1A). Firstly, 20 µL of 3 $mg \cdot mL^{-1}$ $ZnFe_2O_4$ NPs suspension was evenly distributed on the ITO electrode and dried in an oven at 37 °C. The $ZnFe_2O_4$ NPs modified ITO electrode was covered with 20 µL mixed solution containing 10mM EDC and 5 mM NHS and then maintained 1 h. Subsequently, the modified electrode was rinsed with the washing solution; 20 µL of probe DNA (pDNA) suspension (1 µM) was casted onto the ITO/$ZnFe_2O_4$/(EDC/NHS) surface under humid condition in the refrigerator at 4 °C for 8 h. The pDNA was conjugated to the prepared electrode by EDC/NHS coupling reaction between the amino group of $ZnFe_2O_4$ and the -COOH group of pDNA. The acquired electrode was referred to as ITO/$ZnFe_2O_4$/(EDC/NHS)/pDNA. Finally, the ITO/$ZnFe_2O_4$/(EDC/NHS)/pDNA was treated with 10 µL of 0.1 mM aqueous MCH solution at 4 °C for 1 h and then it was washed with the washing solution to obtain the biosensor.

1.5. Hybridization process and detection procedure: 500 µL of biotin modified capture DNA (cDNA) suspension (2 µM) was incubated with 500 µL of Strep-HRP solutions (2 $\mu g \cdot mL^{-1}$) for

30 min at 4 °C to prepare HRP-cDNA via the interaction between biotin and streptavidin. Herein, the DNA molecule labeled with biotin, the molar ratio of DNA to biotin was 1:1. In the HRP-labeled streptavidin, the molar ratio of HRP to streptavidin was also 1:1. One molecule of streptavidin could bind four molecules of biotin. It was speculated that one HRP molecule might bind four DNA molecules. Therefore, the number of DNA molecules per HRP enzyme could be quantitatively controlled by the interaction of streptavidin and biotin during the synthetic reaction. Next, the obtained HRP-cDNA was mixed with certain concentrations of target DNA (tDNA) in the buffer solution. Then an ITO/$ZnFe_2O_4$/(EDC/NHS)/pDNA/MCH electrode was incubated with 20 μL of hybridization buffer solution containing HRP-cDNA and certain concentrations of tDNA at 4 °C for 1 h, washing with the washing solution to obtain ITO/$ZnFe_2O_4$/(EDC/NHS)/pDNA/MCH/(HRP-cDNA/tDNA) (Fig. S1B). It should be pointed out that there was no direct interaction between HRP and $ZnFe_2O_4$. HRP itself had huge steric hindrance. MCH acted as a blocking agent could block the nonspecific sites of $ZnFe_2O_4$ and prevented the adsorption of HRP on $ZnFe_2O_4$. Herein, HRP and $ZnFe_2O_4$ were connected via DNA as a bridge. In the end, the prepared electrode was placed in Tris-HCl buffered solution (0.1 M, pH 7.4) containing 100 μM of H_2O_2 and 500 μM of ABTS for colorimetric assay and PEC determination. In the colorimetric analysis, after incubating at 37 °C for 1 h, the buffered solution with ABTS and H_2O_2 as substrates was monitored by UV-vis spectrometer for colorimetric measurement. In the PEC measurement, the prepared same electrode was placed in Tris-HCl buffered solution (0.1 M, pH 7.4) containing 100 μM of H_2O_2 and 500 μM of ABTS at a PEC workstation for PEC detection. All PEC tests were operated under an excited light source of 470 nm, an applied voltage at -0.05 V, unless otherwise stated. Degassing with high-purity nitrogen for 30 minutes before the experiment, and the nitrogen atmosphere was kept over the solution throughout the experiment.

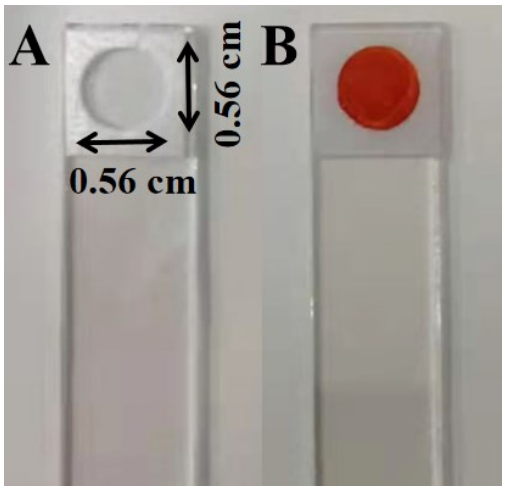

Fig. S1 Photographs of (A) bare ITO electrode and (B) ITO/$ZnFe_2O_4$/(EDC/NHS)/pDNA/MCH/(HRP-cDNA/tDNA) electrode.

2. Results and discussion

2.1. Characterization:

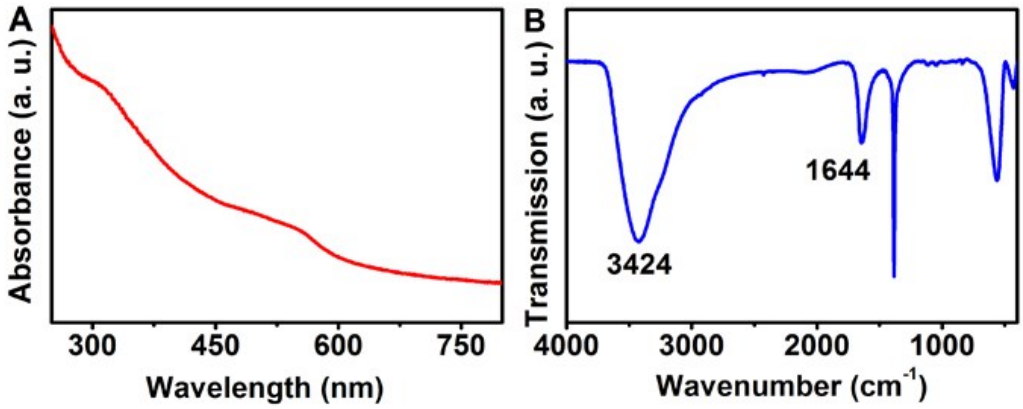

Fig. S2 (A) UV-vis absorption and (B) IR spectra of $ZnFe_2O_4$ NPs.

UV-vis spectroscopy was operated to investigate the optical performance of $ZnFe_2O_4$ NPs, which was due to that the optical absorption of the $ZnFe_2O_4$ NPs could affect the application to PEC biosensing. The absorption spectrum of $ZnFe_2O_4$ NPs revealed an obvious shoulder peak around 470 nm (Fig. S2A), which was consistent with the previous report.[1,2] The occurrence of shoulder peak suggested that $ZnFe_2O_4$ NPs had intensive absorption at approximately 470 nm, which might facilitate the generation of photoinduced electron transfer under the illumination

of a 470 nm light source. In order to make $ZnFe_2O_4$ NPs connect to DNA, $ZnFe_2O_4$ NPs were aminated during the synthesis. Fourier transform infrared (FTIR) test was used to characterize the amino groups on the surface of the $ZnFe_2O_4$ NPs, and the result was shown in Fig. S2B. The amino group (3424 cm^{-1}, 1644 cm^{-1}) appeared on the infrared spectrum of the $ZnFe_2O_4$ NPs,[3,4] indicating that the amino group was successfully leaded to the surface of $ZnFe_2O_4$ NPs. The introduced amino group was used to link the -COOH group of pDNA by EDC/NHS coupling reaction, which was convenient for the preparation of the proposed biosensor.

The fitting result of the Zn 2p XPS spectrum was displayed in Fig. S3A. The peaks at 1022.6 eV and 1045.7 eV were well allocated to Zn $2p_{3/2}$ and Zn $2p_{1/2}$, which indicated Zn (II) was in the $ZnFe_2O_4$ NPs.[5] The other two peaks were located at the binding energies of 1020.9 and 1044.0 eV, which might be attributed to divalent Zn.[6] The fitting result of the O 1s XPS spectrum was exhibited in Fig. S3B. The peak at 529.8 eV corresponded to lattice oxygen of the $ZnFe_2O_4$ NPs, the peak at 531.3 eV and 532.4 eV were assigned to deficient oxygen and surface chemisorbed oxygen.[5,6] The above results indicated that the $ZnFe_2O_4$ NPs were successfully synthesized.

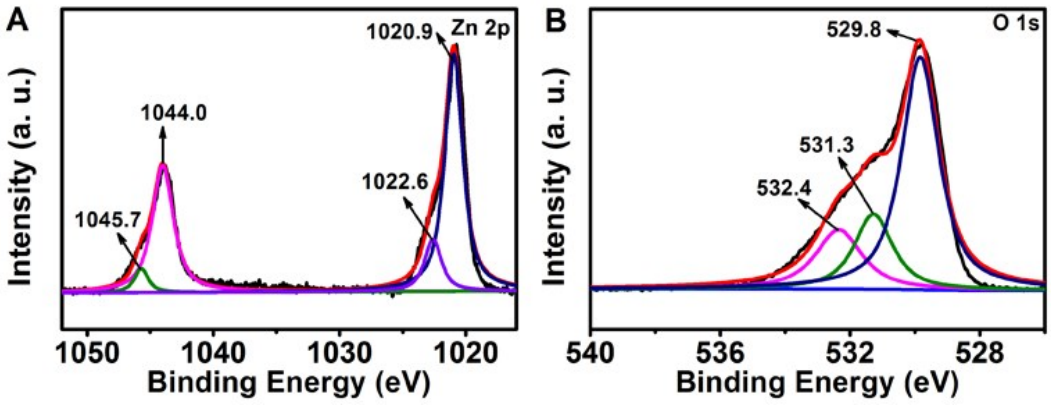

Fig. S3 XPS survey spectra of $ZnFe_2O_4$ NPs for (A) Zn 2p and (B) O 1s.

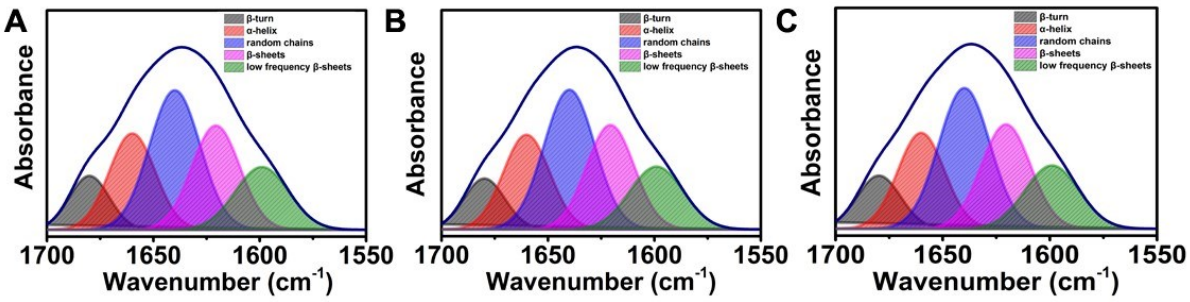

Fig. S4 Deconvoluted FTIR spectra of (A) HRP, (B) HRP-cDNA and (C) $ZnFe_2O_4$/(EDC/NHS)/pDNA/MCH/(HRP-cDNA/tDNA) in the amide I region.

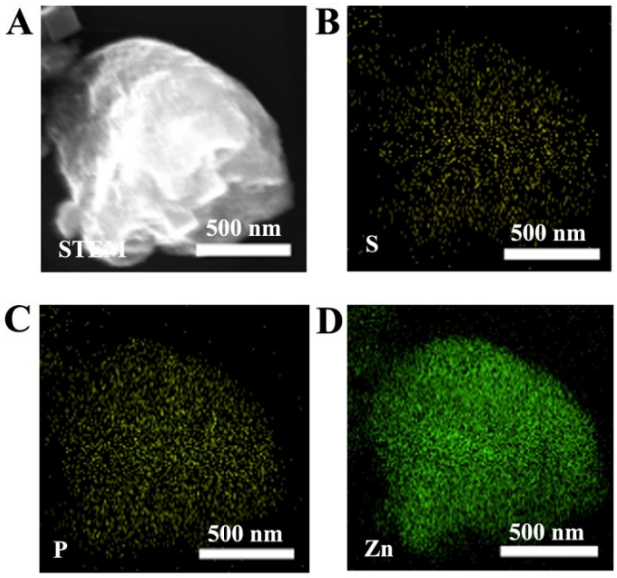

Fig. S5 (A) Element-resolved STEM image of the self-assembled $ZnFe_2O_4$/(EDC/NHS)/pDNA/MCH/(HRP-cDNA/tDNA) and the elemental mapping images for (B) S, (C) P and (D) Zn.

STEM and elemental mapping were applied to characterize the final structure of the $ZnFe_2O_4$/(EDC/NHS)/pDNA/MCH/(HRP-cDNA/tDNA). The results of STEM and elemental mapping images revealed the successful connection of HRP with DNA and $ZnFe_2O_4$ NPs by quantifying the elemental contribution of S (only found in HRP), P (only found in DNA) and Zn (only found in $ZnFe_2O_4$ NPs) related to the total signal (Fig. S5), which indicated the

formation of $ZnFe_2O_4$/(EDC/NHS)/pDNA/MCH/(HRP-cDNA/tDNA).

2.2. The possible mechanism: The natural enzyme (HRP) played a major role in colorimetric analysis, catalyzing the substrates ABTS and H_2O_2 to promote the occurrence of discoloration. Nevertheless, under the effect of visible light irradiation and applied potential, the natural enzyme HRP could not separate electrons and holes, while the separation of electrons and holes of the nanozyme ($ZnFe_2O_4$) was accelerated and its catalytic activity increased (Fig. 2C). The Fe (II) contained in $ZnFe_2O_4$ NPs could undergo redox reaction with H_2O_2, thus $ZnFe_2O_4$ NPs has the activity of catalyzing H_2O_2.[7] Moreover, $ZnFe_2O_4$ NPs possess a good visible light response, excellent photochemical stability, playing a major role in PEC field.[8,9] Electrons are transferred from the electrode to the valence band of the $ZnFe_2O_4$ NPs, and then activated by visible light to transition to the conduction band, generating a cathode photocurrent. H_2O_2 in solution as electron acceptors could effectively increase the photocurrent. Thus, H_2O_2 can be utilized as not only the reactant of the enzyme-catalyzed reaction but also the electron acceptor of the $ZnFe_2O_4$ NPs.[10] HRP and $ZnFe_2O_4$ NPs were integrated and modified on a common platform, the natural enzyme (HRP) played a major role in the colorimetric mode. HRP on the electrode surface would produce the enormous steric hindrance in the PEC mode, which obstructed the transfer of interface electrons and electron acceptors to the electrode surface. Moreover, H_2O_2 was consumed by HRP, and the mechanism may be as follows:[11] HRP + H_2O_2 → HRP-H_2O_2 → HRP-O + H_2O. Therefore, HRP would reduce the photoelectric signal in the PEC mode. In summary, H_2O_2 and HRP promoted the generation of discoloration in the colorimetric mode, while H_2O_2 combined with $ZnFe_2O_4$ NPs in the PEC mode increased the photocurrent intensity. Therefore, using tDNA as the model analyte, through H_2O_2 as a dual-modal switching common regulator, a dual-modal biosensing platform for colorimetry and PEC were established (Scheme S1).

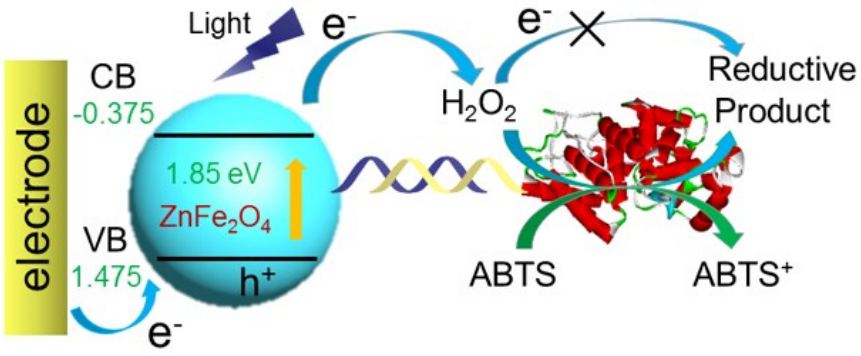

Scheme S1 Schematic illustration of the possible mechanism of the dual-modal colorimetric and PEC biosensing strategy.

2.3. PEC behaviors and EIS of the modified electrodes: Although DNA can act as a molecular wire, almost no photocurrent could be observed on HRP-cDNA modified ITO electrode (Fig. S6, curve b), which was similar with that on HRP modified ITO electrode (Fig. S6, curve a). HRP was not a semiconductor and it could not generate photo-induced electron to produce photocurrent under irradiation. Moreover, HRP itself had huge steric hindrance for the access of photo-induced electron to the electrode surface. Therefore, it was inferred that HRP might not favor the electron transfer to the electrode surface.

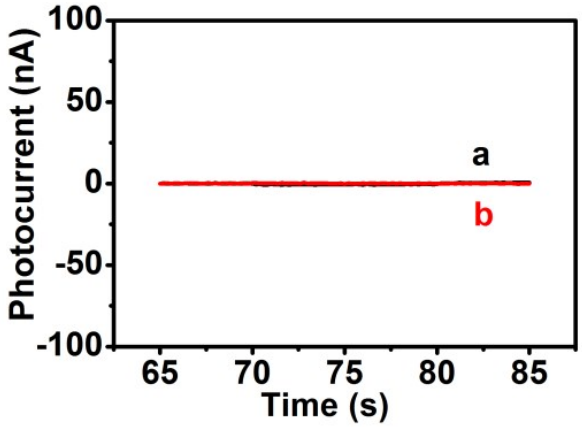

Fig. S6 The PEC responses of (a) HRP (1 μg·mL^{-1}) and (b) HRP-cDNA (500 μL of biotin modified capture DNA (cDNA) suspension (2 μM) was incubated with 500 μL of Strep-HRP solutions (2 μg·mL^{-1}) for 30 min) modified ITO electrodes in 0.1 M Tris-HCl (pH 7.4) containing 100 μM H_2O_2 and 500 μM ABTS.

The layered modification process of our proposed biosensor was characterized by EIS. As displayed in Fig. S7A, EIS included a semicircular part and a straight part, and the diameter of the semicircle was equivalent to the electron transfer resistance (R_{et}). The bare ITO electrode itself performed only a very small semicircle diameter (Fig. S7A, curve a). After the $ZnFe_2O_4$ NPs were applied to the ITO electrode, a slightly larger semicircular (Fig. S7A, curve b) was presented on the EIS, suggesting that $ZnFe_2O_4$ NPs had been immobilized onto the electrode surface. Subsequently, EDC and NHS were mixed to activate the amino group on the $ZnFe_2O_4$ NPs and R_{et} increased (Fig. S7A, curve c), attributing to the unfavorable electronic conductivity of EDC and NHS. When pDNA was introduced, R_{et} further promoted (Fig. S7A, curve d). The negative charges on phosphate backbone of the pDNA blocked the transfer of negatively charged probe ($[Fe(CN)_6]^{3-/4-}$) to the electrode surface owing to the electrostatic repulsion, confirming the immobilization of pDNA on the surface of $ZnFe_2O_4$ NPs.[12] Following blocking with MCH, R_{et} dramatically improved (Fig. S7A, curve e), because its insulation might prevent the redox probe from accessing the electrode surface of electrode. While a mixed solution of the HRP-cDNA and tDNA (5 fM) was applied to the surface, R_{et} enhanced ulteriorly (Fig. S7A, curve f). The more negative charges on phosphate backbone for double-stranded DNA obviously obstructed the transfer of negatively charged redox probe to the surface of electrode owing to the enhanced electrostatic repulsion, verifying that pDNA had been hybridized with HRP-cDNA or tDNA to form double-stranded DNA. The stepwise enhancement of R_{et} via layer-by-layer assembly revealed the successful preparation of PEC biosensor.

The PEC behaviors of the modified electrodes were examined in Tris-HCl (0.1 M, pH 7.4) containing 100 μM H_2O_2 and 500 μM ABTS to assist to prove the assembly processes (Fig. S7B), which was utilized to illustrate the feasibility of the PEC biosensing platform. A very slight photocurrent response (cathodic photocurrent of -0.519 nA) was observed on the bare ITO electrode (Fig. S7B, curve a). Nevertheless, by modifying the $ZnFe_2O_4$ NPs with a narrow band gap and favorable PEC stability,[8,9] the ITO/$ZnFe_2O_4$ electrode generated a remarkable

PEC photocurrent (cathodic photocurrent of -248 nA) (Fig. S7B, curve b) that was 478-fold that of the bare ITO electrode. The improved PEC response could mainly attribute to the formation of electron-hole pairs and effective charge separation of $ZnFe_2O_4$ NPs. Additionally, $ZnFe_2O_4$ NPs could catalyze H_2O_2. H_2O_2 as the electron acceptor controlled electron-hole pairs recombination in $ZnFe_2O_4$ NPs,[13-15] which could promote photoelectric conversion efficiency of $ZnFe_2O_4$ NPs in the visible light region, causing the PEC signal to be amplified. Subsequently, since EDC and NHS could prevent photoexcited electron transfer between $ZnFe_2O_4$ NPs and the electrode, EDC and NHS were mixed to activate the amino group on the $ZnFe_2O_4$ NPs, and the photocurrent reduced to -202 nA (decreased by 18.5%) (Fig. S7B, curve c). With the assembly of pDNA (Fig. S7B, curve d) and blocking with MCH (Fig. S7B, curve e), the photocurrent gradually decreased as the steric resistance of the modified film increased, which obstructed the transport of photo-induced electron and the diffusion of electron acceptor to conduction band of $ZnFe_2O_4$ NPs. After applying a mixed solution of Strep-HRP labeled cDNA and tDNA (5 fM) to the biosensing interface, the photocurrent signal decreased significantly to -105 nA (decreased by 57.5%) (Fig. S7B, curve f), which was owing to the enormous steric hindrance of HRP as a protein dramatically impeded the transfer of interfacial electron and electron acceptor to the electrode surface. With increasing the concentration of tDNA to 100 fM, an improved photocurrent of -158 nA was observed (Fig. S7B, curve g), which was 1.5 times higher than that of tDNA concentration of 5 fM (Fig. S7B, curve f). While the concentration of tDNA promoted, the concentration of Strep-HRP labeled cDNA hybridized with pDNA decreased, owing to a competitive reaction between tDNA and Strep-HRP labeled cDNA. The tDNA completely matched with pDNA, which was better complementary than Strep-HRP labeled cDNA. The decrease of HRP in double-stranded DNA on the electrode surface would facilitate the transfer of interface electrons and electron acceptors to the electrode surface, resulting in a wonderful promotion of the PEC response. Because of the remarkable improvement of photocurrent intensity, a signal-on PEC biosensing strategy could be developed

for DNA detection. Moreover, upon added HRP (Fig. S10, curve a), compared with that of the bare ITO electrode in the absence of HRP (Fig. S7B, curve a), no obviously enhanced photocurrent was observed, suggesting that HRP could not improve photocurrent response in this PEC measurement system. However, the photocurrent intensity with $ZnFe_2O_4$ NPs significantly increased (Fig. S10, curve b) compared with that without $ZnFe_2O_4$ NPs (Fig. S10, curve a), which indicated that $ZnFe_2O_4$ NPs contained the ability to catalyze H_2O_2 which acted as the electron acceptor,[15] thus increasing the PEC response. This phenomenon further verified $ZnFe_2O_4$ NPs rather than HRP could be the main factor of promoting the photocurrent intensity in this PEC test system.

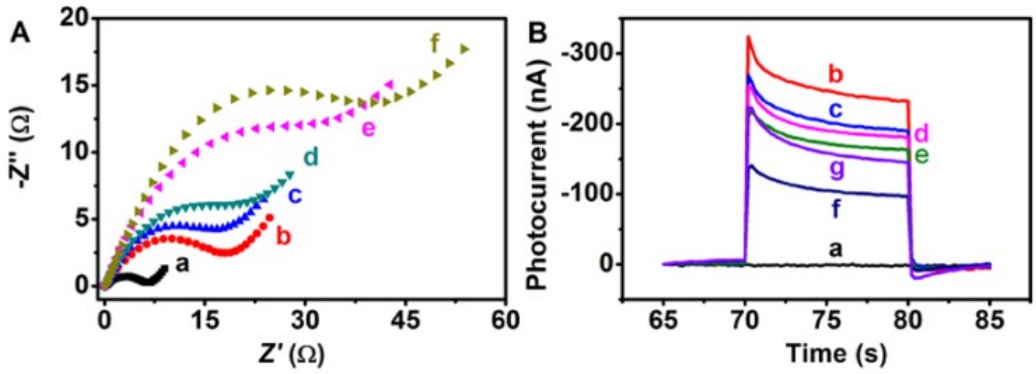

Fig. S7 (A) Nyquist diagrams and (B) PEC responses of (a) bare ITO, (b) ITO/$ZnFe_2O_4$, (c) ITO/$ZnFe_2O_4$/(EDC/NHS), (d) ITO/$ZnFe_2O_4$/(EDC/NHS)/pDNA, (e) ITO/$ZnFe_2O_4$/(EDC/NHS)/pDNA/MCH, (f) ITO/$ZnFe_2O_4$/(EDC/NHS)/pDNA/MCH/(HRP-cDNA/tDNA) (5 fM) and (g) ITO/$ZnFe_2O_4$/(EDC/NHS)/pDNA/MCH/(HRP-cDNA/tDNA) (1×10^2 fM).

2.4. Optimization of conditions for PEC detection: To achieve the goal of designing DNA sensors with excellent PEC performance, several crucial experimental parameters were optimized (Fig. S8). The excitation wavelength was a significant factor affecting the photocurrent signal. As shown in Fig. S8A, the photocurrent intensity reached a maximum at 470 nm, which might be attributed to an intensive absorption of $ZnFe_2O_4$ NPs and the display

of a shoulder peak of UV-vis spectrum at approximately 470 nm (Fig. S2A). The photocurrent excited by the 470 nm light source exhibited powerful enough, which would satisfy the sensitivity required for PEC detection. Therefore, 470 nm was chosen as the excitation wavelength of the PEC biosensor.

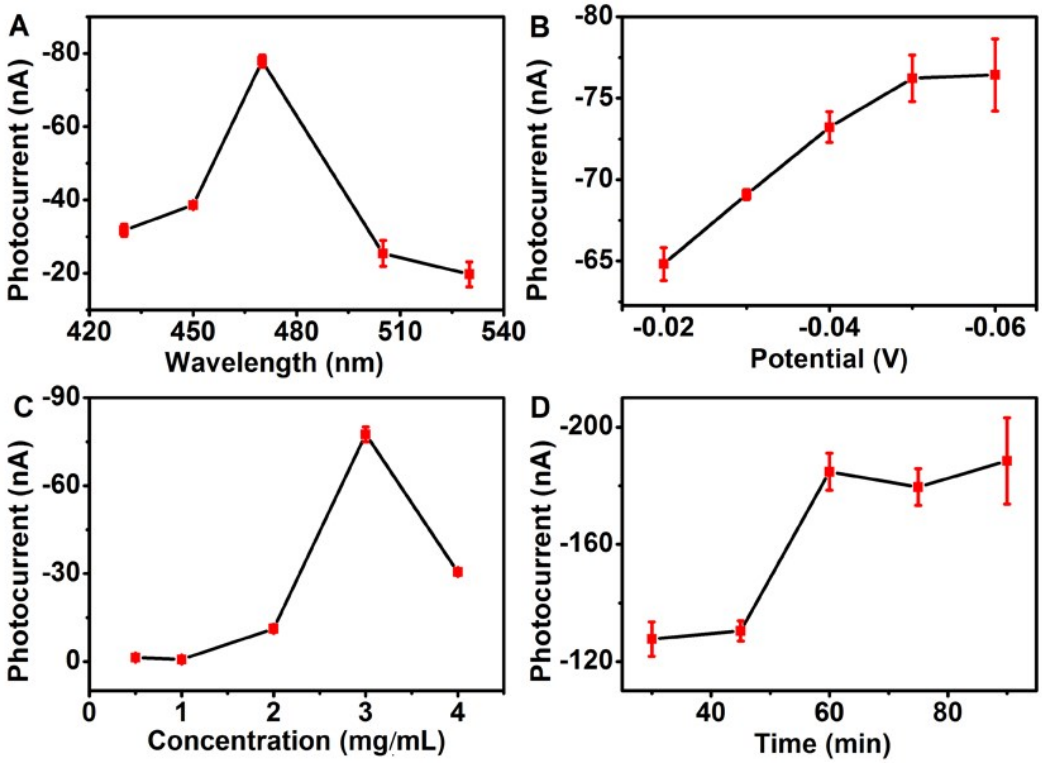

Fig. S8 Effects of (A) excitation wavelength and (B) applied potential and (C) $ZnFe_2O_4$ NPs concentration on photocurrent response of $ZnFe_2O_4$ NPs modified ITO electrode in 0.1 M Tris-HCl (pH 7.4); (D) influence of incubation time on photocurrent response of the PEC biosensor towards tDNA (1×10^3 fM) in 0.1 M Tris-HCl (pH 7.4) containing 100 μM H_2O_2 and 500 μM ABTS.

The bias voltage was another key factor in PEC measurement (Fig. S8B). Under the illumination of the 470 nm light source, the photocurrent promoted from -0.02 V to -0.05 V and then reached a plateau after -0.05 V. The lower bias voltage means the less damage to the biomolecules. Moreover, a low bias voltage could facilitate the elimination of interference from

coexisting materials in the sample. Considering the two aspects, -0.05 V as the applied potential was selected in this PEC test system.

As a PEC biosensing substrate, $ZnFe_2O_4$ NPs were a significant part of the PEC biosensing platform, which directly affected the intensity of photocurrent. When the concentration of $ZnFe_2O_4$ NPs increased from 0.5 to 3 $mg \cdot mL^{-1}$, the photocurrent signal gradually increased, but fell sharply after 3 $mg \cdot mL^{-1}$ (Fig. S8C). The excessive thickness of decorated membranes could obstruct the access of photoinduced electron between $ZnFe_2O_4$ NPs and the electrode. Therefore, 3 $mg \cdot mL^{-1}$ was the optimum concentration for PEC measurement.

The hybridization time of DNA was also a crucial parameter for influencing the photocurrent intensity. The photocurrent signal gently enhanced from 30 to 45 min and then sharply promoted from 45 to 60 min (Fig. S8D). However, when the incubation time exceeded 60 min, the photocurrent signal leveled off, indicating the equilibrium of the hybridization reaction. Consequently, the incubation time for PEC biosensing was fixed at 60 min.

2.5 PEC responses of the modified electrodes:

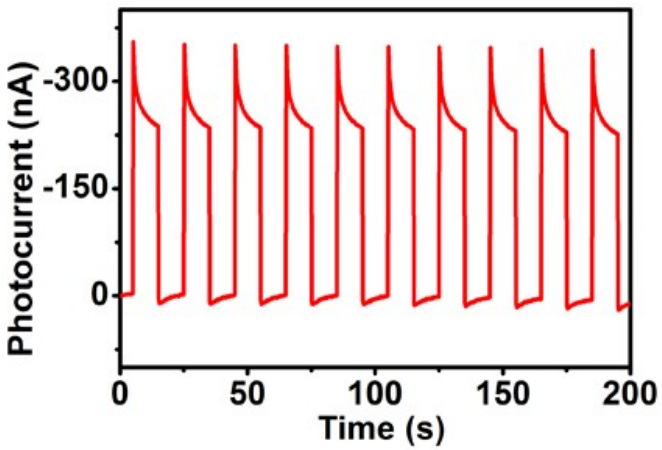

Fig. S9 The PEC response of $ZnFe_2O_4$ NPs modified ITO electrode in 0.1 M Tris-HCl (pH 7.4) containing 100 μM H_2O_2 and 500 μM ABTS.

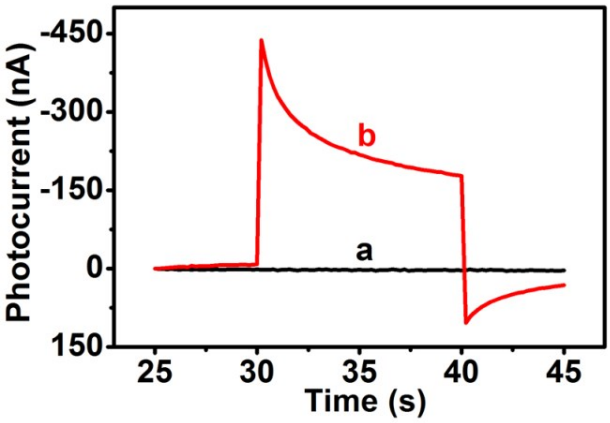

Fig. S10 The PEC responses of (a) the bare ITO electrode and (b) $ZnFe_2O_4$ NPs modified ITO electrode in 0.1 M Tris-HCl (pH 7.4) containing 100 μM H_2O_2, 500 μM ABTS and 1 ng·mL^{-1} Strep-HRP.

2.6. Comparison of the biosensing performance:

Table S1 Comparison of the proposed PEC biosensor with other reported works for DNA detection.

Analytical method	Detection limit	Linear ranger	Reference
Colorimetric	5 pM	10 pM - 500 pM	16
Colorimetric	1 pM	10 pM - 1 nM	17
Fluorescence	5 nM	5 nM - 100 nM	18
Fluorescence	0.5 nM	5 nM - 400 nM	19
Electrochemical	0.12 pM	0.5 pM - 80 pM	20
Electrochemical	3 fM	0.01 pM - 10 nM	21
Colorimetric	0.058 nM	0.5 nM - 5 nM	This work
PEC	0.4 fM	0.5 fM - 1 nM	This work

2.7. Anti-interference ability for PEC detection: The anti-interference ability of the proposed biosensor was investigated with the complementary target DNA, single-base mismatched DNA,

two-base mismatched DNA, and non-complementary DNA. The change of photocurrent responses ΔI ($\Delta I = I - I_0$, where I expressed the photocurrent intensity at different DNA and I_0 was the photocurrent intensity when the concentration of tDNA was zero) for the PEC biosensor hybridized with different targets was explored (Fig. S11). At the same concentration and experimental conditions, the variations of photocurrent responses ΔI of S1 (column b), S2 (column c) and S3 (column d) were merely 53.7%, 29.0% and 20.1% of the PEC signal change of tDNA (column a), respectively, suggesting negligible interference of base mismatch. Furthermore, the level of mismatch discrimination ability was superior to other hybridization-based DNA biosensor,[22] which might be attributed to the enormous steric hindrance of HRP as a protein immobilized on the cDNA would hinder base mismatched DNA to hybridize with pDNA during the competitive reaction and could make them difficult to form double helix structure. These results confirmed that except complementary target DNA, none of the other three DNA species significantly altered the PEC response, indicating a satisfactory specificity for DNA determination.

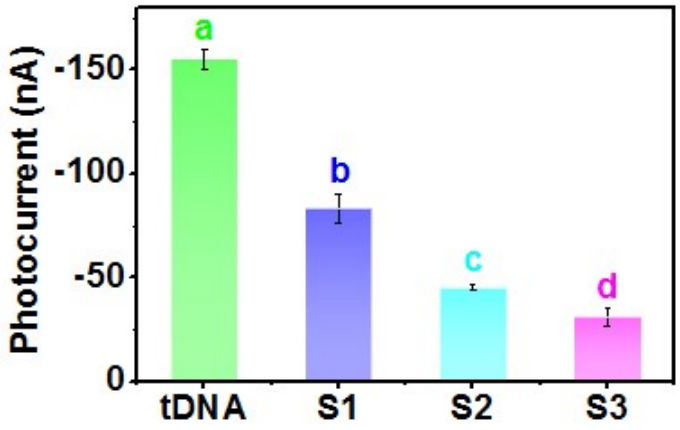

Fig. S11 The change of photocurrent responses (ΔI) for the PEC biosensor hybridized with (a) complementary target DNA (tDNA), (b) single-base mismatched DNA (S1), (c) two-base mismatched DNA (S2) and (d) non-complementary DNA (S3) in 0.1 M Tris-HCl (pH 7.4) containing 100 μM H_2O_2 and 500 μM ABTS. The concentrations of all DNA were 1×10^5 fM.

3. References

1 K. Xiong, K. Z. Wang, L. Chen, X. Q. Wang, Q. B. Fan, J. Courtois, Y. L. Liu, X. G. Tuo and M. H. Yan, *Nano-Micro Lett.*, 2018, **10**, 17.

2 X. D. Zhu, N. Guijarro, Y. P. Liu, P. Schouwink, R. A. Wells, F. Le Formal, S. Sun, C. Gao and K. Sivula, *Adv. Mater.*, 2018, **30**, 1801612.

3 X. H. Liu, J. Zhang, L. W. Wang, T. L. Yang, X. Z. Guo, S. H. Wu and S. R. Wang, *J. Mater. Chem.*, 2011, **21**, 349−356.

4 J. H. Muyonga, C. G. B. Cole and K. G. Duodu, *Food Chem.*, 2004, **86**, 325−332.

5 L. R. Hou, L. Lian, L. H. Zhang, G. Pang, C. Z. Yuan and X. G. Zhang, *Adv. Funct. Mater.*, 2015, **25**, 238−246.

6 L. Lv, Y. L. Wang, P. F. Cheng, B. Zhang, F. Dang and L. P. Xu, *Sens. Actuator B-Chem.*, 2019, **297**, 126755.

7 Y. W. Pan, M. H. Zhou, Q. Wang, J. J. Cai, Y. S. Tian and Y. Zhang, *J. Hazard. Mater.*, 2020, **391**, 122210.

8 S. Y. Cao, X. Q. Yan, Z. Kang, Q. J. Liang, X. Q. Liao and Y. Zhang, *Nano Energy*, 2016, **24**, 25−31.

9 I. N. Reddy, C. V. Reddy, A. Sreedhar, J. Shim, M. Cho, K. Yoo, D. Kim and J. S. Gwag, *J. Electroanal. Chem.*, 2018, **823**, 517−526.

10 W. W. Zhao, J. J. Xu and H. Y. Chen, *Biosens. Bioelectron.*, 2017, **92**, 294−304.

11 Y. F. Zhang and H. Hess, *Anal. Chem.*, 2020, **92**, 1502−1510.

12 L. Yuan, W. W. Tu, J. C. Bao and Z. H. Dai, *Anal. Chem.*, 2015, **87**, 686−692.

13 L. Y. Ning, X. L. Guan, J. W. Ma, M. Wang, X. B. Fan, G. L. Zhang, F. B. Zhang, W. C. Peng and Y. Li, *J. Alloy. Compd.*, 2018, **738**, 317−322.

14 L. Shen, C. C. Chu, C. Ma, H. M. Yang, S. G. Ge, J. H. Yu, M. Yan and X. R. Song, *Sens. Actuator B-Chem.*, 2014, **201**, 196−203.

15 W. Y. Liu, H. M. Yang, Y. A. Ding, S. G. Ge, J. H. Yu, M. Yan and X. R. Song, *Analyst*, 2014, **139**, 251−258.

16 J. Y. Dai, H. F. He, Z. J. Duan, Y. Guo and D. Xiao, *Anal. Chem.*, 2017, **89**, 11971−11975.

17 E. Hosseinzadeh, H. Ravan, A. Mohammadi and H. Pourghadamyari, *Talanta*, 2020, **216**, 120913.

18 W. J. Zhou, J. B. Zhu, D. Q. Fan, Y. Teng, X. Q. Zhu and S. J. Dong, *Adv. Funct. Mater.*, 2017, **27**, 1704092.

19 Y. Teng, X. F. Jia, S. Zhang, J. B. Zhu and E. K. Wang, *Chem. Commun.*, 2016, **52**, 1721−1724.

20 E. H. Xiong, Z. Z. Li, X. H. Zhang, J. W. Zhou, X. X. Yan, Y. Q. Liu and J. H. Chen, *Anal. Chem.*, 2017, **89**, 8830−8835.

21 D. Wang, Y. Q. Chai, Y. L. Yuan and R. Yuan, *Anal. Chem.*, 2019, **91**, 3561−3566.

22 Y. H. Wang, H. H. Shi, K. Cui, L. N. Zhang, S. G. Ge, M. Yan and J. H. Yu, *Biosens. Bioelectron.*, 2018, **117**, 515−521.